Nuclear Inst. and Methods in Physics Research, A 979 (2020) 164383

Contents lists available at ScienceDirect

Nuclear Inst. and Methods in Physics Research, A

journal homepage: www.elsevier.com/locate/nima

LGAD designs for Future Particle Trackers

N. Cartiglia [a,*], R. Arcidiacono [a,b], G. Borghi [e,f], M. Boscardin [e,f], M. Costa [a,d], Z. Galloway [c], F. Fausti [a,d,1], M. Ferrero [a,b], F. Ficorella [e,f], M. Mandurrino [a], S. Mazza [c], E.J. Olave [a,d], G. Paternoster [e,f], F. Siviero [a,d], H. F-W. Sadrozinski [c], V. Sola [a,d], A. Staiano [a], A. Seiden [c], M. Tornago [a,d], Y. Zhao [c]

[a] INFN, Torino, Italy
[b] Università del Piemonte Orientale, Italy
[c] SCIPP, University of California Santa Cruz, CA, USA
[d] Università di Torino, Torino, Italy
[e] Fondazione Bruno Kessler, Trento, Italy
[f] TIFPA-INFN, via Sommarive 18, 38123, Povo (TN), Italy

ARTICLE INFO

Keywords:
Silicon
Fast detector
Low gain
Charge multiplication
LGAD

ABSTRACT

Several future high-energy physics facilities are currently being planned. The proposed projects include high energy e^+e^- circular and linear colliders, hadron colliders, and muon colliders, while the Electron–Ion Collider (EIC) is expected to construct at the Brookhaven National Laboratory in the future. Each proposal has its advantages and disadvantages in terms of readiness, cost, schedule, and physics reach, and each proposal requires the design and production of specific new detectors. This paper first presents the performances necessary for future silicon tracking systems at the various new facilities. Then it illustrates a few possibilities for the realization of such silicon trackers. The challenges posed by the future facilities require a new family of silicon detectors, where features such as impact ionization, radiation damage saturation, charge sharing, and analog read-out are exploited to meet these new demands.

1. Introduction

Several future facilities of high-energy physics have presently been considered, with a timescale of 15–30 years. The proposals consider accelerators for e^+e^-, hadrons, muons, and electron–ions. The requirements for silicon trackers differ mostly upon the type of particles that are accelerated, and not on the specifics of a given proposal. For examples, at the various e^+e^- machines (Circular Electron Positron Collider — CPEC, Compact Linear Collider — CLIC, Future Circular Collider — FCC-ee, and International Linear Collider — ILC) the key requests are about low material budget and excellent spatial resolution, with modest requests for radiation resistance or precise timing (σ_t < 50 ps). On the other hand, at hadron machines (Future Circular Collider — FCC-hh, High Energy LHC — HE-LHC, and Super Proton Proton Collider — SppC) the most challenging requests are the radiation resistance (fluences above $1 \cdot 10^{17}$ n_{eq}/cm^2) and the spatial and time precision (pileup ∼ 1000 events/bunch crossing, σ_t ∼ 5 ps/hit, σ_x ∼ 5 μm/hit). The requests for the muon collider are similar to those of CLIC, however, plus a time resolution of ∼ 50 ps for the inner tracker and ∼ 100 ps for the outer tracker. Table 1, taken from [1], summarizes the present requirements for the silicon trackers at various facilities, while an updated review has been presented at the TREDI 2020 conference [2]. There are several possible paths to future silicon trackers [1,3], including HVCMOS, low field monolithic sensors, and hybrid detectors. In the following part of this paper, three key aspects of LGAD design evolution for future silicon trackers will be considered: (i) extension of picosecond time resolution to fluences above the present limit of $1–2 \cdot 10^{15}$ n_{eq}/cm^2, (ii) design of silicon sensors able to withstand fluences in the range $1–10 \cdot 10^{16}$ n_{eq}/cm^2, and (iii) capability of obtaining excellent position resolution without increasing the channel count dramatically. The technological challenges presented are connected to the design of the silicon sensors. However, it is essential to stress the importance of the interconnection with the front-end electronics: silicon sensors and associated electronics succeed or fail together. In [4], the evolution of 3D sensors to meet the requirement of 4D tracking is presented: equivalently to the present situation of silicon trackers, 3D sensors will be crucial to cover the area with the most extreme fluence levels. The present contribution will not develop further on this topic.

* Corresponding author.
E-mail address: cartiglia@to.infn.it (N. Cartiglia).
[1] Now at DE.TEC.TOR. Devices & Technologies Torino S.r.l., Torino, Italy.

https://doi.org/10.1016/j.nima.2020.164383
Received 26 March 2020; Received in revised form 3 May 2020; Accepted 22 May 2020
Available online 18 July 2020

Table 1
Summary of the parameters of future silicon trackers at new facilities.

	HL-LHC	SPS	FCC-hh	FCC-ee	CLIC	$\mu\mu$ Col.
Fluence [$n_{eq}/cm^2/y$]	10^{16}	10^{17}	10^{17}	$< 10^{10}$	$< 10^{11}$	
Hit rate [$s^{-1}cm^{-2}$]	2–4G	8G	20 G	20 M	240 k	
Inn. tracker [m^2]	10	0.2	15	1	1	
Out. tracker [m^2]	200	–	400	200	140	
Pixel size [μm^2]	50 × 50	50 × 50	25 × 50	25 × 25	25 × 25	
Time res [ps]	50	40	10	1k	5k	50–100

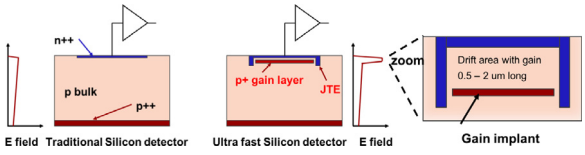

Fig. 1. Key layout features of an n-in-p silicon sensor (left side) and of an UFSD (center). The right side shows an expanded view of the multiplication region.

2. Extension of UFSD picosecond time resolution to fluences above the present limit of 1–2·10^{15} n_{eq}/cm^2

In the last five years, silicon detectors have gone from being considered unfit to perform accurate timing measurement to be the only viable solution for the construction of large tracker detectors performing the simultaneous measurements of space and time, the so-called 4D-tracking system [5]. This change of paradigm was brought about by the introduction of low gain avalanche diodes (LGAD) [6] and their subsequent design optimization for timing application (Ultra Fast Silicon Detector, UFSD) [7]. Fig. 1 illustrates the key technical steps of this evolution: to the design of a traditional n-in-p sensor, left side of the picture, an additional deep p-implant has been added (central part of the picture). In the region between this implant and the n^{++} read-out electrode, the electric field is high enough (right side of the picture) for generating multiplication of the drifting electrons. Presently, LGAD are manufactured by several foundries, including CNM (Spain) [8], FBK (Italy) [9], Hamamatsu [10] (Japan), Micron (England), BNL [11] (USA), and NDL [12] (China).

The defining feature of the UFSD design, the deep p^{++} implant, responsible for generating the high E-field needed to create controlled multiplication, has, at the moment, a radiation resistance limited to fluences of about 1–2·10^{15} n_{eq}/cm^2. The underlying reason for this effect is the acceptor removal mechanism [13,14] that decreases the doping density of the gain layer to a level where it does not any longer generate a high-enough field. In the past three years, there has been extensive development in the understanding of the acceptor removal mechanism and the design of UFSD with enhanced resistance to radiation. Fig. 2 reports this progress by showing the active fraction of the gain layer as a function of fluence for two typical FBK UFSD productions, one from 2016 and one from 2019. The key technical difference between the two outputs is the infusion of carbon in the gain layer, which reduces the acceptor removal mechanism [15,16]. If we consider the limit of the radiation resistance as the value at which the gain layer decreases by 20%, between the 2016 and 2019 productions, there is an improvement of a factor of 4, from 4·10^{14} n_{eq}/cm^2 to 1.5·10^{15} n_{eq}/cm^2. This increase is mostly due to the carbon infusion and a better design of the gain layer. The 20% value is based on experimental measurements [17–19] demonstrating that, for reductions below this value, the electric field in the gain layer is too low to be restored by an increase of the detector bias.

There are several UFSD productions planned for the next few years, in conjunction with the ATLAS [20] and CMS [21] timing layer and for R&D studies (mostly in connection with the CERN RD50 activities [22]). There are presently two paths that exploring how to improve the UFSD radiation resistance: (i) decreasing the acceptor removal rate and (ii) enhancing the recovery capability of the bias voltage. The first

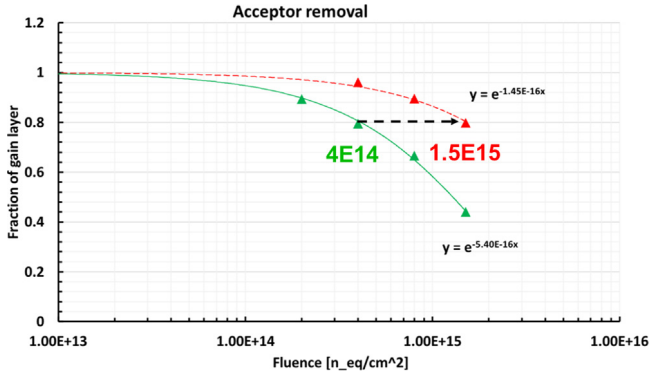

Fig. 2. Active fraction of gain layer in UFSD as a function of irradiation. The green curve represents the typical behavior for prototypes manufactured in 2016 while the red curve for those manufactured by FBK in 2018 with carbon infusion. (For interpretation of the references to color in this figure legend, the reader is referred to the web version of this article.)

idea, increasing the gain layer radiation resistance, has actively been pursed by FBK with the production of UFSD wafers using a varying density of infused carbon. In the 2019 FBK UFSD3 production, the density of carbon infusion used in the 2018 UFSD2 production has been increased by a factor of 2, 3, and 5, without finding any improvement in radiation resistance [9]. In the 2020 UFSD3.2 production, the density of carbon infusion has been reduced to 80% and 40% of that of UFSD2. This production will, therefore, complete the scan in carbon density and will help pinpoint the dose of carbon infusion that maximizes the radiation resistance. Acceptor removal can be decreased by the addition of different elements, besides carbon: the RD50 collaboration is pursuing this path by investigating the microscopic mechanism of acceptor removal and modeling the beneficial effects of carbon.

The second technique to increase the radiation resistance of the UFSD design is to enhance the recovery capability of the bias voltage. In UFSD, as radiation deactivates the gain layer, the electric field in the gain region is kept high by increasing the bias voltage. The field per micron is linear with the bias voltage and inversely proportional to the sensor thickness, $E = Bias/Thickness$. One obvious choice is to make the sensor thinner: a bias increase of 100 Volt in a 25 μm thick sensor increases the field by 4 V/μm while only by 1 V/μm in a 100 μm thick sensor. The obvious drawbacks of this choice are that thin sensors have higher capacitance and generate a small signal. Another option is to design the gain layer such that the bias voltage increase has a more substantial impact on charge multiplication [23]. Charge multiplication happens in the space between the gain layer and the n^{++} read-out electrode, right panel of Fig. 1. The gain G is defined as

$$G \propto e^{\alpha(E,T)\cdot d} \quad with \quad \alpha(E,T) \propto e^{-(a+b\cdot T)/E} \tag{1}$$

where d is the total distance and $\alpha(E,T)$ the impact ionization coefficient, function of the field E, and the temperature T via the two experimental parameters a, b. $\lambda = 1/\alpha$, represents the length to achieve $G = e$. The ratio d/λ determines the gain: if two gain layers are implanted at different depths, d_1, d_2, they will achieve the same gain when $d_1/\lambda_1 = d_2/\lambda_2$. Fig. 3, top panel, shows the dependence of λ upon the field, according to the Massey impact ionization model [24]:

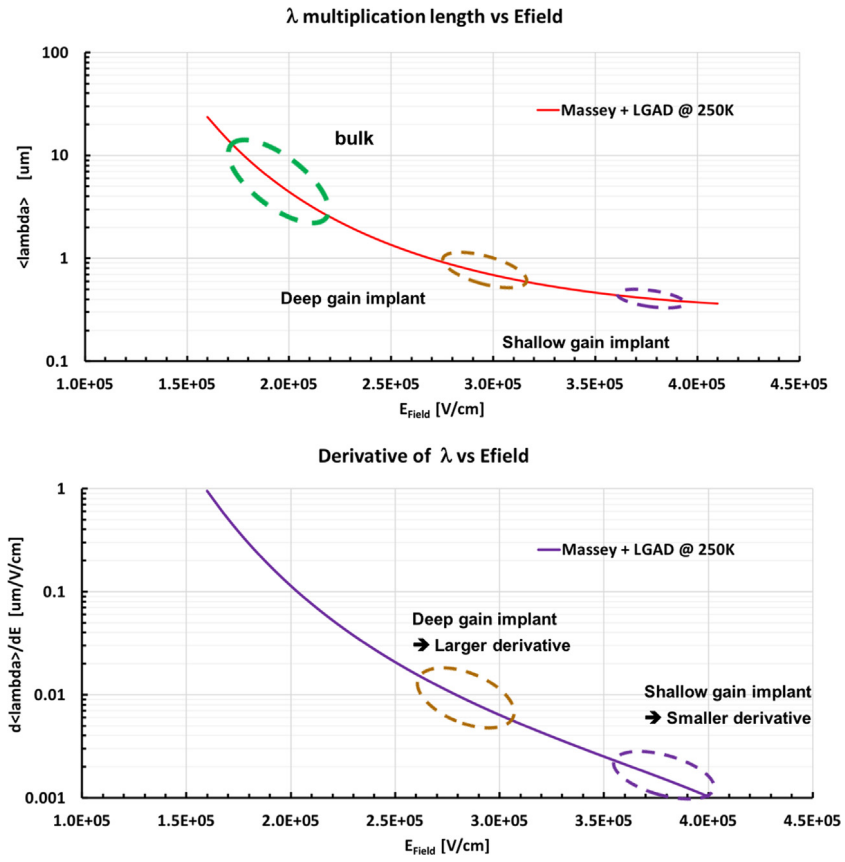

Fig. 3. Top: multiplication length λ as a function of the electric field. Bottom: derivative of the multiplication length as a function of the electric field.

in deeper gain layer designs, the drift length d is longer and the electric field lower than for shallower gain layer. The restoration power of the bias voltage is evaluated by studying the derivative $d\lambda/dE$, shown at the bottom panel of Fig. 3. For very high fields, i.e., shallow gain layer, the derivative is very small, indicating that a significant increase in bias is necessary to restore the field needed for multiplication. In contrast, for a deeper gain layer, a much lower increase is necessary. For sensors with a deep gain layer, the recovering effect of the bias voltage is therefore much higher than for those with a shallow gain layer. The recovering power of the bias voltage for varying temperatures (the gain goes down as the temperature goes up) has confirmed this effect. Sensors with deep gain layers require a voltage increase of 1 V/°C to keep the gain constant while sensors with shallow gain layer require almost an increment of 2 V/°C (the coefficient b is therefore different in the two cases). Two additional considerations on deep gain layers: (i) they need a lower doping density, and therefore are more prone to the acceptor removal mechanism, (ii) since the multiplication happens at lower field values, the excess noise factor is reduced, potentially leading to better timing performances.

The 2020 FBK UFSD3.2 production will explore the combination of carbon infusion with a deep gain layer.

The different aspects presented in this section point to a potential extension of the radiation hardness of UFSD, hopefully above fluences of $5{\cdot}10^{15}$ n_{eq}/cm^2.

3. Exploitation of radiation damage saturation in the design of silicon sensors for fluences above $1{\cdot}10^{16}$ n_{eq}/cm^2

In the last few years, a set of novel measurements on highly irradiated sensors (fluences $\sim 1{\cdot}10^{17}$ n_{eq}/cm^2) have demonstrated that silicon sensors behave better after heavy irradiation than what was predicted by extrapolating lower fluence data ($\phi < 1{\cdot}10^{15}$ n_{eq}/cm^2) to higher values [25–27]. Fig. 4 (taken from [28] and reference therein) exemplifies this saturation effect for three different parameters: the leakage current, the trapping probability, and the creation of acceptor-like states.

As the three panels show, the initial linear dependence of the damage with fluence becomes a logarithmic trend at larger fluence. The reason for this change is not understood. A naive consideration is that after a fluence of $1{\cdot}10^{15}$ n_{eq}/cm^2 every single silicon lattice cell has been traversed by a particle: for fluences above $1{\cdot}10^{15}$ n_{eq}/cm^2, radiation damage happens to already damaged cells and, possibly, damage on damaged silicon has fewer consequences. The exploitation of saturation effects is the key to the design of silicon sensors able to work at fluences about $1{\cdot}10^{17}$ n_{eq}/cm^2: our current understanding is that, once the saturation effects are included, thin sensors will continue to work. Even after $1{\cdot}10^{17}$ n_{eq}/cm^2 the changes to thin silicon sensors (20–30 μm) are not dramatic: the leakage current is quite low, the charge collection efficiency is high and the full depletion voltage, $V_{FD} = e|N_{eff}|x^2/2\epsilon$, where N_{eff} is the bulk doping and x the detector thickness, remains below 500–600 V. The drawback of thin sensors is that the generated signal is too low: present state-of-the-art ASICs, for example, those produced for HL-LHC, require a minimum charge of about 1 fC [29]. This problem could be solved by using sensors with internal gain; however, gain in very irradiated sensors has not been studied enough to know if this approach might or might not work. Impact ionization in thin sensors should happen in the bulk, at relatively low fields, as indicated in Fig. 3. In the current models of impact ionization available in TCAD,[2] the impact ionization coefficient α does not have an explicit dependence upon the fluence ϕ. However, it can be added by simply duplicating the dependence upon temperature:

$$\alpha(E,T) \propto e^{-(a+b\cdot T)/E} \rightarrow \alpha(E,T,\phi) \propto e^{-(a+b\cdot T+c\cdot\phi)/E}. \quad (2)$$

[2] www.synopsys.com/silicon/tcad.html.

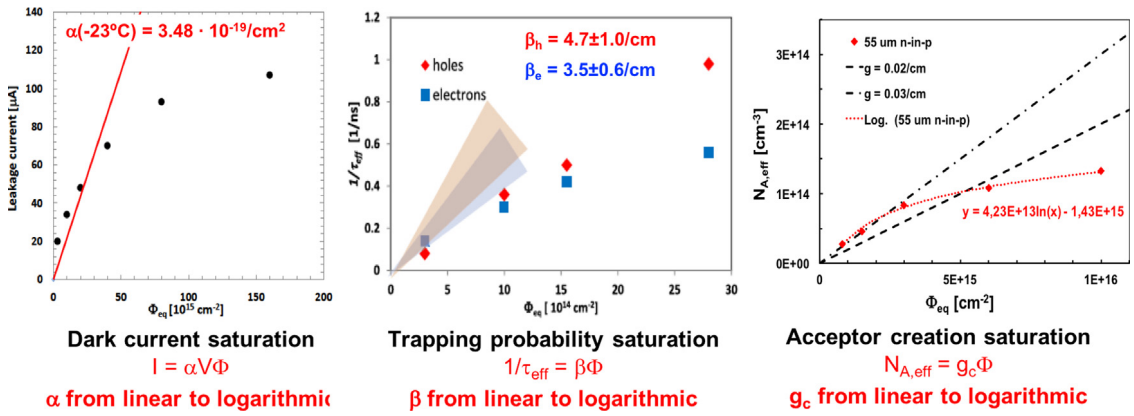

Fig. 4. Radiation damage in silicon sensors as a function of fluence: the leakage current, the trapping probability, and the creation of acceptor-like states show clear signs of saturation.

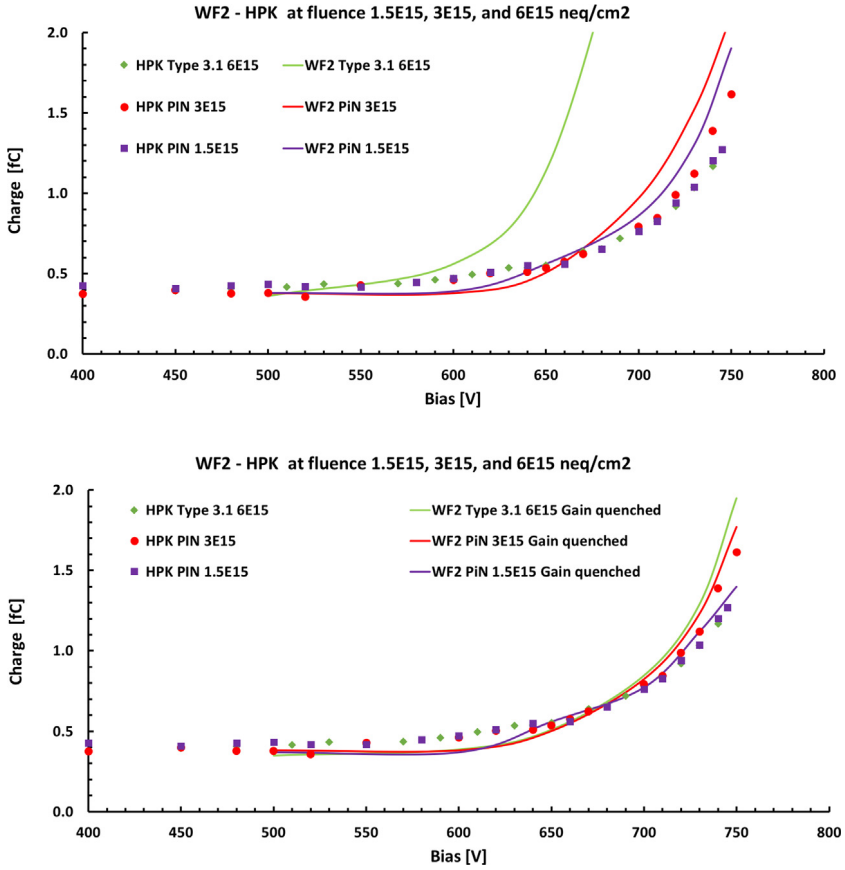

Fig. 5. Signal integral in 45 μm thick HPK sensor as a function of the bias voltage for three irradiation levels. The solid curve shows the predicted charge without (top) and with (bottom) gain quenching.

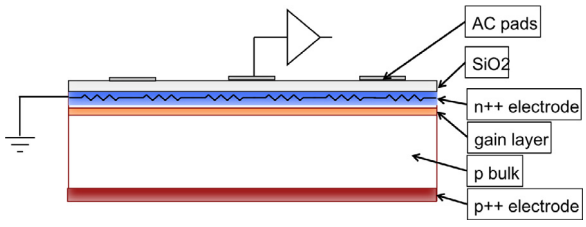

Fig. 6. Schematic of an AC-LGAD sensor.

The effect of the coefficient c in Eq. (2) is to decrease the gain as the fluence increases; it is a gain-quenching term that accounts for the presence of additional scattering centers in damaged silicon. As an initial study, the multiplication in the sensor bulk has been investigated for HPK 45 μm thick sensors, irradiated up to $6{\cdot}10^{15}$ n_{eq}/cm^2 and compared with the Massey impact ionization model as implemented in the Weightfield2 (WF2) simulation program [30]. The top side of Fig. 5 shows the collected signal as a function of bias voltage for 3 fluences (1.5, 3, and $6{\cdot}10^{15}$ n_{eq}/cm^2), together with the prediction of WF2. The signal is generated by a 1064 nm pico laser, tuned to provide the same charge as the MPV of an impinging MIP. Note that the sensor irradiated at $6{\cdot}10^{15}$ n_{eq}/cm^2 is a UFSD, and the leftover gain from the gain layer is taken into account in the simulation. The gain simulation,

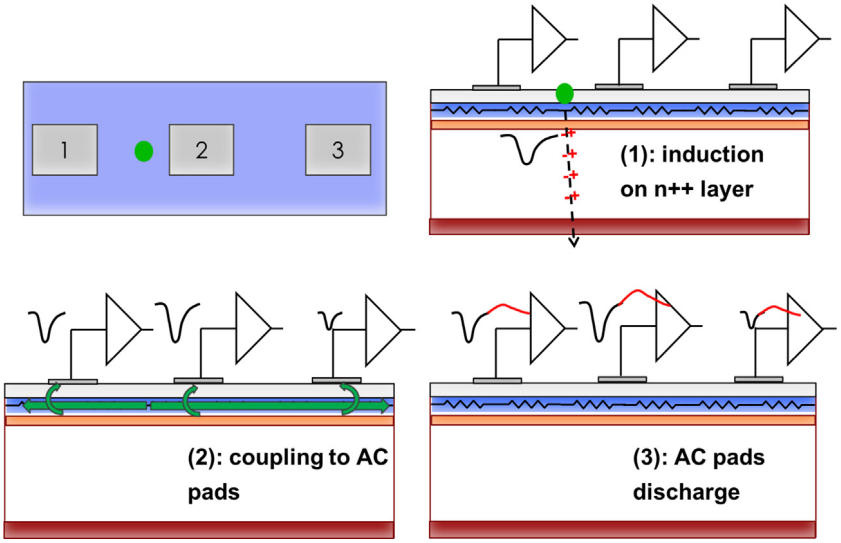

Fig. 7. Signal formation in AC-LGAD: the signal is seen on the electrodes with a delay proportional to the distance from the impinging point indicating that the formation mechanism is not direct induction.

in the absence of gain quenching ($c = 0$), predicts an increasing gain with fluence, driven by the field generated by the bulk doping. This prediction is clearly not supported by the data, Fig. 5 top panel. The simulation can be reconciled with the data introducing a quenching mechanism, as proposed in Eq. (2), with $c = 2 * 10^{-11} V/\phi$. With this addition, the simulation and the data agree quite well, Fig. 5 bottom. This study demonstrates that gain is still present after a fluence of $6{\cdot}10^{15}$ n_{eq}/cm^2, albeit already quenched. The investigation of gain in thin sensors will continue in the next years by irradiating even thinner sensors (20–30 μm), where bulk multiplication might be less affected by lattice defects since it is achieved at a higher field and lower λ.

Overall, radiation damage saturation suggests the possibility of using thin sensors for future FCC-hh trackers for position measurements; future studies of impact ionization in heavily irradiated sensors will shed light on the feasibility of this idea. The possibility of the accurate timing measurement at fluences above $1{\cdot}10^{16}$ n_{eq}/cm^2 is much more complicated, as it requires large signals and small noise, and it might not be possible with this technology.

4. Charge sharing as a solution for excellent position resolution without using very small pixels

Good position resolution is achieved by designing sensors with small pixels: in binary read-out, the resolution is normally quoted as $bin\ size/\sqrt{12}$. The proposed future detectors, listed in Table 1, have pixel sizes from 50×50 to 25×25 μm^2. The need for excellent position resolution drives such a high granularity. However, it is not otherwise necessary since the occupancy is low (this is not the case for FCC-hh). Charge sharing between pads yields to a much more precise localization of the hit; however, the e/h drift lines in traditional pixel detectors are such that analog sharing is limited. Charge sharing in silicon sensors can be obtained by designing a new type of device where the signal on the read-out pads is not induced (following Ramo's theorem) during the drift of the e/h charge carriers in the bulk, but it is picked up in AC coupled mode during the propagation of the signal towards ground. AC-coupled LGADs [31,32] are designed on this principle, maximizing charge sharing between pads to obtain a position resolution a factor of 5–10 better than $bin\ size/\sqrt{12}$. AC-coupled LGAD, Fig. 6, are n-in-p sensors, with a continuous gain layer, a resistive n^{++} implant, and a thin dielectric layer for AC coupled read-out. The size of the AC metal pads determines the read-out segmentation, and it can be adjusted to any geometry by simply changing two production masks (metal etching and overglass), leaving the rest of the sensor identical. The goal of the resistive n^{++} layer is to keep the signal localized, to reduce the capacitance seen by the read-out pad, and to induce the AC signal on the metal pad, somewhat equivalent to the role of the graphite layer in Resistive Plate Chambers (RPC)[3] [33,34]. For this reason, AC-LGADs are also called *resistive silicon detector* (RSD). AC-LGADs were produced by CNM in 2017 [32], by FBK within the RSD project [35,36], and by BNL [37].

Signal formation in AC-LGAD happens in the 3 phases [38] sketched in Fig. 7: (i) The first step is similar to all other silicon sensors: the drift of the e/h pairs generates an induced signal on the n^{++}electrode. Note that there is no direct induction on the metal pads, the n^{++} is conductive enough to stop it. (ii) The signal spreads laterally along the lossy transmission line composed by the n^{++} layer and the bulk and AC capacitance. The metal pads act as pick-up electrodes and record a signal. (iii) In the last phase, the AC pads discharge, with an RC that depends on the read-out input resistance, the n^{++} sheet resistance, and the capacitance of the system.

The signal is seen on the AC pads with a delay and an attenuation that depends on the distance from the impinging point, as it is reported in Fig. 8. The closest pad, marked in red, sees the earliest and largest signal, while the black pad the smallest and the most delayed one. The signal is composed of a first lobe, with a shape very similar to that of a standard LGAD, followed by a second lobe, longer and with opposite polarity. Other important aspects of the signal in AC-LGAD: (i) when summing up all pads, the total amplitude is almost constant regardless of the impinging particle position, (ii) signal attenuation is higher for sensors with a large fraction of the area covered by metal, attenuation $\propto (metal/pitch)^2$, (iii) the signal delay is about 0.5–1.5 ps/μm, (iv) the signal of particles hitting a metal pad is not shared if the metal pad is wider than 80–100 μm^2.

In AC-LGAD, the measurement of the arrival time and hit position exploits the mechanism of charge sharing between multiple pads explained above, reaching concurrent very good time ($\sigma_t \sim$ 20–30 ps) and position ($\sigma_x \sim$ 10 μm) resolutions. AC-LGADs are, therefore, able to achieve a position precision that far exceeds that of binary read-out, allowing a strong reduction of the read-out channels. As a matter of comparison, a 200 μm pitch AC-LGAD has the same spatial resolution of a 25 μm pitch traditional sensors. In a hybrid configuration, this fact

[3] RPCs consist of two electrode plates, both made from a resistive material with metal contacts on the external part, separated by a thin layer of gas. When a charged particle ionizes the gas molecules, the electrons/ions travel towards the electrodes, and AC-coupled signals are seen on the metal contacts.

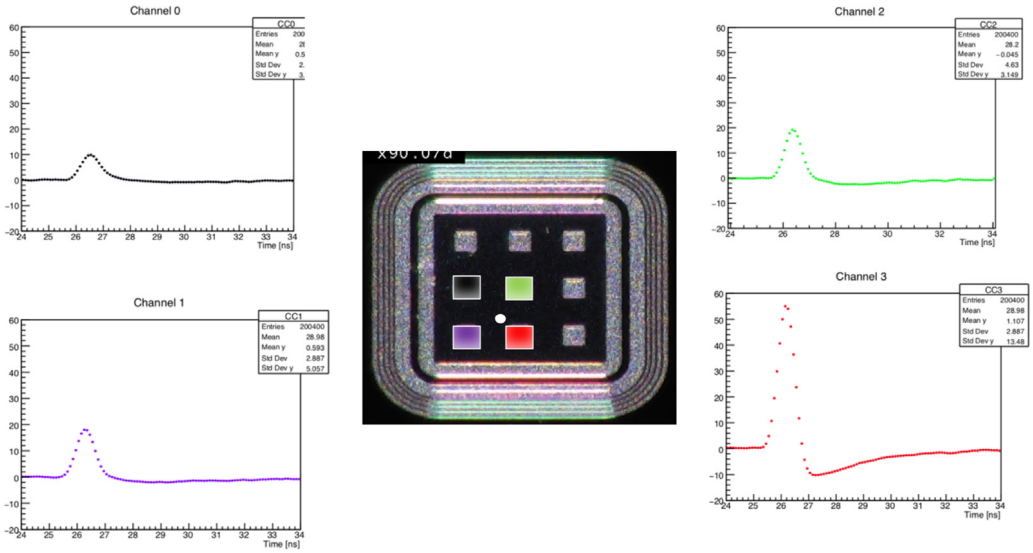

Fig. 8. Example of signal sharing among 4 pads in AC-LGAD (RSD) sensors: the signal is delayed and attenuated with distance. This result has been obtained by placing an RSD detector on a multi-channel read-out board, and shining on the sensor light pulses generated by a 1064 nm picolaser. The signal traces are read-out using a 4-channel, 4 GHz, 20GS/s digital oscilloscope. (For interpretation of the references to color in this figure legend, the reader is referred to the web version of this article.)

has significant consequences as it reduces the number of channels by a factor of ~ 50, it allows using more power per channel, and it provides a lot more available area per read-out channel. More results on AC-LGAD (RSD) are presented in [9,39].

5. Conclusions and outlook

The characteristics of the silicon tracking detectors proposed for the new accelerator facilities are extremely challenging in terms of radiation resistance, spatial and time resolution, power consumption, area, and material budget. An intense R&D phase is necessary to meet these challenges, together with new ideas in the design of the detectors. Internal gain, introduced in the mainstream silicon design a few years ago with the advent of the LGAD architecture, coupled with the exploitation of the saturation of radiation damage, measured in the last few years, has the potentiality to help to achieve these goals. A new design of silicon detector, the so-called AC-LGAD (RSD) architecture, uses charge sharing to achieve the excellent time and spatial resolutions required by the new silicon trackers while reducing the number of channels by more than a factor of 10. In the next few years, the performance of AC-LGADs will be measured, and their design optimized. Given the continuous gain layer, the AC-LGAD design is also very promising for 4D tracking at small pitch sizes with a 100% fill factor.

Declaration of competing interest

The authors declare that they have no known competing financial interests or personal relationships that could have appeared to influence the work reported in this paper.

Acknowledgments

We thank our collaborators within RD50, ATLAS, and CMS, who participated in the development of UFSD. Part of this work has been financed by the European Union Horizon 2020 Research and Innovation funding program, under Grant Agreement no. 654168 (AIDA-2020) and Grant Agreement no. 669529 (ERC UFSD669529), and the MIUR, Italy via the Dipartimento di Eccellenza, Physics Dep. of Torino (ex L. 232/2016, art. 1, cc. 314, 337). The work was supported by the United States Department of Energy, grant DE-FG02-04ER41286.

References

[1] M. Aleksa, et al., Strategic RD Programme on Technologies for Future Experiments, Tech. Rep. CERN-OPEN-2018-006, CERN, Geneva, 2018, URL https://cds.cern.ch/record/2649646.

[2] E. Sicking, Detector requirements for future high-energy collider experiments, 2020, [online] TREDI2020.

[3] M. Munker, et al., Vertex and tracking detector R&D for CLIC, in: Proceedings of the 12th International "Hiroshima" Symposium, HSTD12, at Hiroshima, Japan, HSTD12, 2019.

[4] A. Lai, et al., Results of the TIMESPOT project on sensors and electronics developments for future vertex detectors, in: Proceedings of the 12th International "Hiroshima" Symposium, HSTD12, at Hiroshima, Japan, HSTD12, 2019.

[5] H.F.-W. Sadrozinski, A. Seiden, N. Cartiglia, 4D tracking with ultra-fast silicon detectors, Rep. Progr. Phys. 81 (2) (2018) 026101, URL http://stacks.iop.org/0034-4885/81/i=2/a=026101.

[6] G. Pellegrini, et al., Technology developments and first measurements of low gain Avalanche detectors (LGAD) for high energy physics applications, Nucl. Instrum. Methods A 765 (2014) 12–16.

[7] N. Cartiglia, et al., Design optimization of ultra-fast silicon detectors, Nucl. Instrum. Methods A 796 (2015) 141–148.

[8] M. Carulla, et al., 50 μm thin low gain avalanche detectors (LGAD) for timing applications, Nucl. Instrum. Methods A A924 (2019) 373–379, http://dx.doi.org/10.1016/j.nima.2018.08.041.

[9] R. Arcidiacono, et al., State-of-the-art and evolution of UFSD sensors design at FBK, in: Proceedings of the 12th International "Hiroshima" Symposium, HSTD12, at Hiroshima, Japan, HSTD12, 2019.

[10] X. Yang, et al., Layout and performance of HPK prototype LGAD sensors for the high granularity timing detector, in: Proceedings of the 12th International "Hiroshima" Symposium, HSTD12, at Hiroshima, Japan, HSTD12, 2019.

[11] G. Giacomini, W. Chen, F. Lanni, A. Tricoli, Development of a technology for the fabrication of low-gain avalanche diodes at BNL, Nucl. Instrum. Methods A A934 (2019) 52–57, http://dx.doi.org/10.1016/j.nima.2019.04.073, arXiv:1811.04152.

[12] Y. Fan, et al., IHEP-NDL prototype LGAD sensors for the HGTD, in: Proceedings of the 12th International "Hiroshima" Symposium, HSTD12, at Hiroshima, Japan, HSTD12, 2019.

[13] H.F.-W. Sadrozinski, et al., In-depth experimental study of acceptor removal in low-gain Avalanche detectors, in: Proceedings of the 12th International "Hiroshima" Symposium, HSTD12, at Hiroshima, Japan, HSTD12, 2019.

[14] G. Kramberger, et al., Radiation effects in low gain avalanche detectors after hadron irradiations, J. Instrum. 10 (07) (2015) P07006, URL http://stacks.iop.org/1748-0221/10/i=07/a=P07006.

[15] M. Ferrero, et al., Radiation resistant LGAD design, Nucl. Instrum. Methods A 919 (2019) 16–26, http://dx.doi.org/10.1016/j.nima.2018.11.121, URL http://www.sciencedirect.com/science/article/pii/S0168900218317741.

[16] M. Moll, et al., Effects of displacement damage involving the shallow acceptor doping in p-type silicon devices, in: Proceedings of Vertex 2019: 28th International Workshop on Vertex Detectors, Vertex19, 2019.

[17] Z. Galloway, et al., Properties of HPK UFSD after neutron irradiation up to 6E15 n/cm^2, 2017, arXiv:1707.04961.

[18] G. Kramberger, et al., Radiation effects in low gain Avalanche detectors after hadron irradiations, J. Instrum. 10 (2015) P07006.
[19] S. Mazza, et al., Proprieties of FBK UFSDs after neutron and proton irradiation up to 6 * 10e15 neq/cm^2, 2018, URL https://arxiv.org/abs/1804.05449.
[20] ATLAS Collaboration, Technical Proposal: A High-Granularity Timing Detector for the ATLAS Phase-II Upgrade, Tech. Rep. CERN-LHCC-2018-023. LHCC-P-012, CERN, Geneva, 2018, URL http://cds.cern.ch/record/2623663.
[21] CMS, A MIP Timing Detector for the CMS Phase-2 Upgrade, Tech. Rep. CERN-LHCC-2019-003. CMS-TDR-020, CERN, Geneva, 2019, URL https://cds.cern.ch/record/2667167.
[22] RD50 Collaboration, Radiation hard semiconductor devices for very high luminosity colliders [online].
[23] N. Cartiglia, A naive parametrization of initial acceptor removal, in: 32th RD50 Workshop, Hamburg, Germany, 2018, URL https://indico.cern.ch/event/719814/contributions/3022722/attachments/1662756/2668052/InitialAccrem.pdf.
[24] D. Massey, et al., Temperature dependence of avalanche multiplication in submicron silicon devices, in: Proceedings of 35th European Solid-State Device Research Conference, ESSDERC 2005, 2005, pp. 245–248.
[25] G. Kramberger, Reasons for high charge collection efficiency of silicon detectors at HL-LHC fluences, Nucl. Instrum. Methods A A924 (2019) 192–197, http://dx.doi.org/10.1016/j.nima.2018.08.034.
[26] N. Cartiglia, H.F.W. Sadrozinski, A. Seiden, Tracking particles at fluences 5-10 ·1E16 n_{eq}/cm^2, Proc. Sci. VERTEX2018 (2019) 029, http://dx.doi.org/10.22323/1.348.0029, arXiv:1908.11605.
[27] I. Mandic, et al., Measurements with Si detectors irradiated to extreme fluences, 2020, [online] TREDI2020.
[28] V. Sola, et al., Next-generation tracking system for future hadron colliders, in: Proceedings of Vertex 2019: 28th International Workshop on Vertex Detectors, Vertex19, 2019.
[29] L. de Maria, et al., Results and perspectives from RD53 on the next generation readout chips for HL-LHC silicon pixel detector phase 2 upgrades, 2019, [online] TREDI2019.
[30] F. Cenna, et al., Weightfield2: A fast simulator for silicon and diamond solid state detector, Nucl. Instrum. Methods A 796 (2015) 149–153, http://dx.doi.org/10.1016/j.nima.2015.04.015, Proceedings of the 10th International Conference on Radiation Effects on Semiconductor Materials Detectors and Devices.
[31] N. Cartiglia, et al., Issues in the design of ultrafast silicon detectors, 2015, [online] Tredi2015.
[32] H. Sadrozinski, et al., Timing resolution measurements on utra-fast silicon detectors, URL indico.cern.ch/event/577879/contributions/2740418/.
[33] R. Santonico, R. Cardarelli, Development of resistive plate counters, Nucl. Instrum. Methods Phys. Res. 187 (2) (1981) 377–380, http://dx.doi.org/10.1016/0029-554X(81)90363-3, URL http://www.sciencedirect.com/science/article/pii/0029554X81903633.
[34] W. Riegler, C. Lippmann, R. Veenhof, Detector physics and simulation of resistive plate chambers, Nucl. Instrum. Methods A 500 (2003) 144–162, http://dx.doi.org/10.1016/S0168-9002(03)00337-1.
[35] M. Mandurrino, et al., Demonstration of 200-, 100-, and 50-µm pitch resistive AC-coupled silicon detectors (RSD) with 100% fill-factor for 4D particle tracking, IEEE Electron Device Lett. 40 (11) (2019) 1780–1783, http://dx.doi.org/10.1109/LED.2019.2943242.
[36] M. Mandurrino, et al., Analysis and numerical design of resistive AC-coupled silicon detectors (RSD) for 4D particle tracking, Nucl. Instrum. Methods A A959 (2020) 163479, http://dx.doi.org/10.1016/j.nima.2020.163479.
[37] G. Giacomini, W. Chen, G. D'Amen, A. Tricoli, Fabrication and performance of AC-coupled LGADs, J. Instrum. 14 (09) (2019) P09004, http://dx.doi.org/10.1088/1748-0221/14/09/P09004,10.1088/1748-0221/14/09/p09004, arXiv:1906.11542.
[38] N. Cartiglia, et al., Signal formation and designed optimization of resistive AC-LGAD (RSD), 2020, [online] TREDI2020.
[39] G. Paternoster, et al., Novel strategies for fine-segmented LGADs, in: Proceedings of the 12th International "Hiroshima" Symposium, HSTD12, at Hiroshima, Japan, HSTD12, 2019.